Letter | Editors' Suggestion

Electronic structure of nitrogen-doped lutetium hydrides

Adam Denchfield,[1] Hyowon Park,[1,2] and Russell J. Hemley[1,3,4]
[1]Department of Physics, University of Illinois Chicago, Chicago, Illinois 60607, USA
[2]Materials Science Division, Argonne National Laboratory, Lemont, Illinois 60439, USA
[3]Department of Chemistry, University of Illinois Chicago, Chicago, Illinois 60607, USA
[4]Department of Earth and Environmental Sciences, University of Illinois Chicago, Chicago, Illinois 60607, USA

(Received 30 May 2023; accepted 23 January 2024; published 16 February 2024)

First-principles density functional theory (DFT) calculations of supercell structures based on N-doped $Fm\bar{3}m$ LuH_3 reveal configurations of $Fm\bar{3}m$ $Lu_8H_{23-x}N$ that exhibit novel electronic properties such as flat bands, sharply peaked densities of states (van Hove singularities, vHs), and intersecting Dirac cones near the Fermi energy (E_F). These electronic properties are present when N substitutes H in the octahedral interstices of $Fm\bar{3}m$ LuH_3. These structures also exhibit an interconnected metallic hydrogen network, a common feature of high-T_c hydride superconductors. Electronic property systematics gives an estimate of T_c for one structure that is well above the critical temperatures predicted for structures considered previously. DFT+U has an especially strong effect on one of the structures considered, enhancing the vHs and flat bands near E_F. These results provide a basis for understanding the electronic properties observed for nitrogen-doped lutetium hydride.

DOI: 10.1103/PhysRevMaterials.8.L021801

Rare-earth hydrides form a unique chemical composition of the heavy rare-earth ions and the lightest hydrogen atoms that can lead to novel material properties including metal-insulator transitions and superconductivity. Such novel properties originate from the subtle balance between the strongly localized nature of heavy electrons in rare-earth ions and the itinerant electronic behaviors of hydrogen. A particularly intriguing example is nitrogen-doped lutetium hydride, which has recently been reported to exhibit near-ambient superconductivity [1]. The disposition and stoichiometry of the light elements are not known, nor is it clear what role, if any, nitrogen plays in the reported superconductivity. First-principles searches have not found structures with strong electron-phonon coupling (EPC) [2–7]. It is of interest to find structures in the ternary Lu-H-N system with strong vHs near the Fermi energy (E_F) in the density of states (DOS) because those features increase EPC [8,9].

Inspired by the pioneering theoretical predictions of high T_c superconductivity by Ashcroft [10,11], density functional theory (DFT) calculations have played an important role in guiding experiments aimed at realizing room temperature superconductivity, specifically in dense hydrides [12,13] with calculations that have been confirmed by subsequent experiments [14–18] (see [19] for a review). The recent report of room-temperature superconductivity in $LuH_{3-x}N_y$ at 1 GPa [1] has motivated numerous recent DFT calculations aimed at understanding the result [1–5,7,20]. Candidate structures and stoichiometries have been identified and proposed, but they do not exhibit properties conducive to known superconducting mechanisms. We use DFT [21–23] and DFT+U [24,25] calculations to explore bonding and electronic properties of a broad range of structures and compositions that fit the available experimental data. We show that a subset of Lu-H-N structures and stoichiometries consistent with available experimental constraints [1] exhibit novel electronic structures that include Dirac cones, a sharp vHs, and flat bands at E_F. These features imply strong EPC and, if stabilized against structural instabilities, may support a high-temperature superconducting phase [26].

We begin our study by computing the electronic structure of a variety of supercells based on $Fm\bar{3}m$ $LuH_{3-x}N_y$ in light of recent theoretical studies of the energetics of the system [2–5,7,20]. In the parent structure $Fm\bar{3}m$ LuH_3, each Lu atom is surrounded by hydrogens in tetrahedral and octahedral sites (Fig. 1, top). Preserving the large electron-phonon coupling of FCC RH_3 [27] suggests only considering a limited nitrogen content. Additionally, the experimental constraints suggest a N:Lu ratio near 1:8 [1] (i.e., $y = 0.125$ in $LuH_{3-x}N_y$) and a highly symmetric structure similar to $Fm\bar{3}m$ LuH_3, which suggests symmetric N-doped supercells of LuH_3. These factors narrowed our search, and $Fm\bar{3}m$ $Lu_8H_{23-x}N$ for small x emerged as particularly important due to its interesting electronic structure.

We consider four main superlattice structure types with stoichiometry $Lu_8H_{23-x}N$ (Fig. 1, bottom). Structure A consists of alternating layers of LuH_3 and type 1 ordering $LuH_{2.75}N_{0.25}$, resulting in a face-centered-cubic (FCC) superlattice of N atoms. Structure B has N in tetrahedral sites (type 2 ordering), and was chosen for study due to predicted stability of compounds with N substituting H in tetrahedral sites [6]. Structures C and D provide examples of electronic properties of the less symmetric structures of the same stoichiometries. Notably, structures A, C, and D have N in octahedral sites. Structure C has an ABCB stacking, where B are LuH_3 layers, and A and C layers are type 1 orderings with a relative shift. Structure D is more complex, but its key feature is N-Lu-N chains. The full structural information is presented in Figs. S1–S5. To study hydrogen vacancies, we present two inequivalent octahedral hydrogen vacancy positions inside the type 1 ordering scheme. The unit cell parameters and atomic

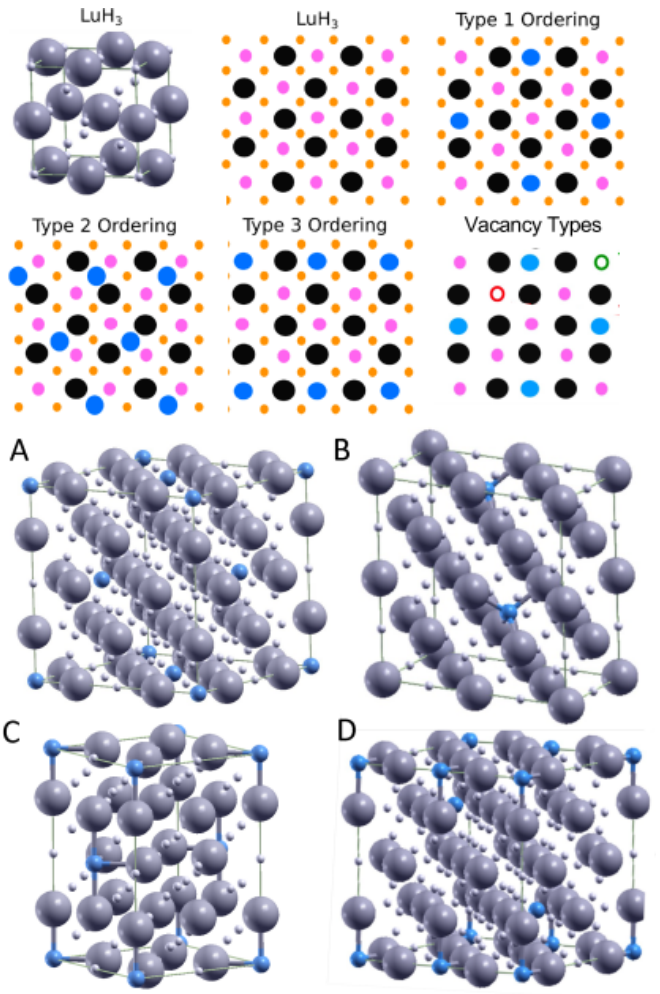

FIG. 1. Top: Unit cell of Fm$\bar{3}$m LuH_3 followed by depictions of the layers [(100) planes] that form the building blocks of the superlattice structures considered in the present study: LuH_3 layer; type 1 ordering, with N in the octahedral site; type 2 ordering, with N in the tetrahedral site; type 3 ordering, with chains of octahedrally coordinated N; and the two types of octahedral H vacancies denoted by open circles (red: type 1, green: type 2), with the tetrahedral hydrogens omitted for clarity. Bottom: the four $2 \times 2 \times 2$ superlattice structure types for $Lu_8H_{23-x}N$ (A, B, C, D) created from the above ordering schemes (see text and Supplemental Material [28]).

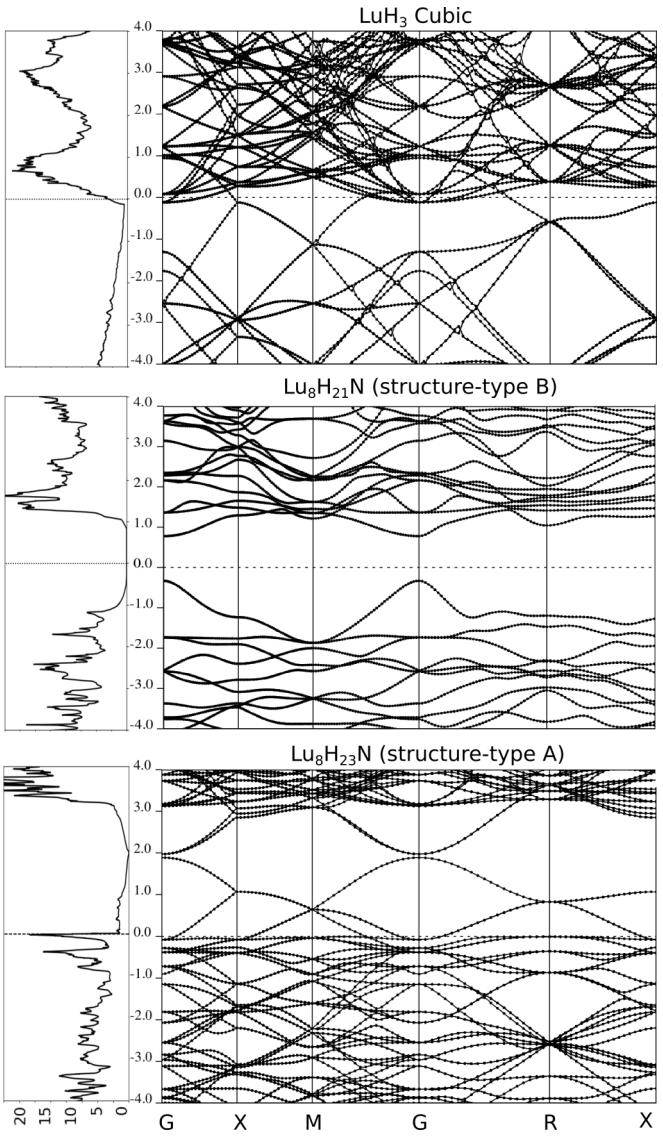

FIG. 2. The band structures of (top) Fm$\bar{3}$m LuH_3, (middle) $Lu_8H_{21}N$ ($Lu_8H_{21}N$ structure-type B) [6], and (bottom) $Lu_8H_{23}N$ (structure-type A) using DFT+U, U=8.2 eV on Lu_d, 5.5 eV on Lu_f.

positions of the superlattice structure-types were relaxed without symmetry (see the SM [28]). When the above structures are relaxed, the Lu atoms move towards the N atoms. The simulated x-ray diffraction patterns of the structures are broadly consistent with those measured experimentally [1] (Fig. S6), with structure A matching the best. However, important superlattice reflections at low angle were not observed because of limitations of the experiment. The optimized lattice parameter of structure A (Fig. S1) at zero pressure with DFT-PBE ($a = 10.03$ Å) is close to twice the value obtained experimentally for the dominant Fm$\bar{3}$m phase in the experiments ($a = 5.023$ Å) [1].

Figure 2 shows the band structures of Fm$\bar{3}$m LuH_3, $Lu_8H_{21}N$ (structure-type B) [6], and $Lu_8H_{23}N$ (structure-type A), the latter using DFT+U (see also Fig. S7). Our computed LuH_3 band structure is in good agreement with the DFT results calculations of Sufyan and Larsson [29] (Fig. S8). $Lu_8H_{21}N$ (B) has a sizable band gap, meaning it cannot be a superconducting phase. Despite the same number of valence electrons, this large difference with LuH_3 is likely due to the stoichiometry rather than differences in tetrahedral vs octahedral site chemistry. Placing N in tetrahedral vs octahedral positions does not significantly alter the DOS, seen by comparing all the PDOS in Figs. S9(a)–9(d). Sun *et al.* [6] examined the stability and properties of $Lu_8H_{21}N$ (B) and found it is not conducive to superconductivity [6], consistent with our calculated band structure. Remarkably, the bands of $Lu_8H_{23}N$ (structure A) are distinctly different, exhibiting a combination of hybridization and correlation effects giving rise to a very sharp vHs at E_F and regions of nearly flat bands (discussed later) with sharp intersecting Dirac cones (Fig. S10).

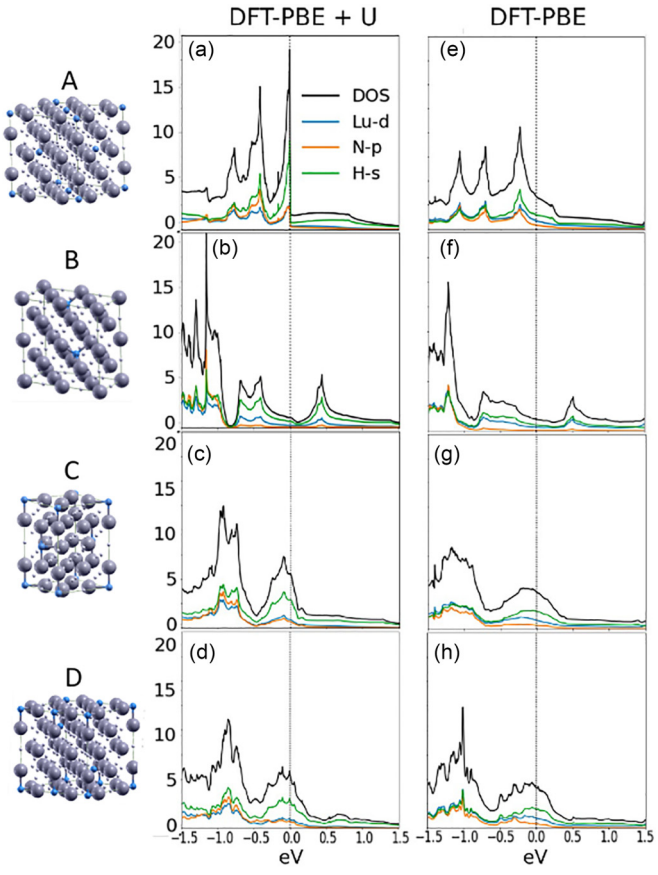

FIG. 3. Calculated PDOS near E_F of superlattice structure types A-D with DFT-PBE+U, U=8.2 eV on Lu_d [30] (a)–(d) vs DFT-PBE (e)–(h).

Figure 3 compares the partial density of states (PDOS) near E_F of these and other structures including both DFT+U and DFT results. We placed U = 8.2 eV on the Lu_d orbitals since the pseudopotentials used are tested for this U value to match accurate (but expensive) HSE06 functional calculations for LuN [30]. Our own DFT+U calculations confirm that this U correctly predicts the LuN band gap at the experimental lattice constant, but it also leads to an overestimation of the lattice constant upon energy minimization with respect to the unit cell parameters (see Table S2 of the SM [28]).

$Lu_8H_{23}N$ (A) exhibits an extraordinarily sharp vHs close to E_F [Fig. 3(a); see also Fig. S7] that is dominated by H_s states with additional contributions from N_p and Lu_d. This feature does not change significantly with U (Fig. S11), indicating our results are broadly valid for a wide range of U. It is known that sharp vHs at E_F lead to T_c estimates that grow unbounded with the DOS at E_F [8,31,32] unlike the flat DOS approximation [33]. $Lu_8H_{23}N$ structures B–D are relatively featureless around E_F [Figs. 3(b)–3(d)] but share similar broad features below E_F and become more similar when unrelaxed (Fig. S9). The crystal field splitting and H_s^{oct}, H_s^{tet} projections for the parent structure LuH_3 and structures A–D are shown in Figs. S7 and S9. We also studied other structures with Lu:N ratios of 1:6, 1:4, and 1:2, and a broad range of hydrogen fillings of the 1:8 ratio. For the most part, the 1:6, 1:4, and 1:2 stoichiometries do not have hydrogen states dominant at E_F, unlike that of the 1:8 structures.

To study the correlation effects in structures A–D we compare the DFT-PBE results in Figs. 3(e)–3(h). The removal of U changes structure A, whose vHs is now broadened and 0.2 eV below E_F [Fig. 3(e)], though it is still sharp compared to hydrides with very high predicted T_c [12] (Fig. S19). The removal of U for the other structures changes their DOS marginally [Figs. 3(f)–3(h)]. The main effect of U for structure A is to push Lu_d states away from E_F (Figs. S11, S16, and S17); near E_F, multiband effects result in an enhancement of the vHs at E_F [Figs. 3(a), S12, S16, and S17].

In all the configurations shown, the hydrogens are the primary contributors at E_F, with additional Lu_d and N_p contributions (Fig. S9). The results contrast with those of Ferreira *et al.* [4] who found only structures with primarily Lu_d character at E_F. Of the structures considered thus far, structure A uniquely responds to the DFT+U with a sharp vHs at E_F. Orbital-projected bandstructures of structure A reveal that the flat bands at E_F are primarily of hydrogen character with some nitrogen hybridization near E_F at L, K, U, and X (Figs. S16 and S17). DFT+U indirectly affects the Lu_d hybridization with the other orbitals, which results in flatter bands closer to E_F. Exploring the effect of introducing vacancies into structure A on the vHs (Fig. S13), we find the electronic structure (vHs) is stable to a small number of octahedral hydrogen vacancies with the effect of raising E_F. This in combination with the hole-doping effect of N atoms on the LuH_3 bands in $Lu_8H_{23}N$ (Fig. S7) can thus tune E_F to match the van Hove singularity peak, an effect that can significantly enhance superconductivity in other materials [9,34]. In addition, the application of modest pressure (i.e., 2 GPa) to $Lu_8H_{23}N$ (A) increases the vHs energy by 13 meV, potentially changing T_c significantly over this range as the vHs goes from below E_F to above it. These options represent a strategy to tune the parameters of $Lu_8H_{23-x}N$ (A) to maximize the achievable T_c.

The total energies of the $Lu_8H_{23}N$ structures considered here (Table S1) are within 7–30 meV/atom of each other. The DFT results are consistent with those reported for $Lu_8H_{23}N$ by Sun *et al.* [6] who also found $Lu_8H_{21}N$ (B) to be dynamically stable. Calculations without U for structure A find the Γ-point phonons to be weakly unstable at ambient, but stable above 10 GPa. This suggests any dynamical instabilities may be stabilized by pressure or anharmonic and nuclear quantum effects, as found for other hydrides [35–38]. We also considered the effects of magnetic properties on the energetics. DFT and DFT+U calculations indicate any magnetic states have small magnetic moments with energies lowered by less than 1 meV/atom, i.e., negligible compared to ambient temperatures.

Figure 4 further illustrates the electronic properties near E_F of $Lu_8H_{23}N$ (A) with DFT-PBE+U. The integrated local density of states (ILDOS) around the Fermi energy shows that the conduction states are composed of octahedral hydrogen and N states, with nontrivial contributions from the tetrahedral hydrogen. A "metallic hydrogen" network forms in the ILDOS (sliced three ways for illustrative purposes) with mostly localized N states; smaller and larger rings of octahedral and tetrahedral hydrogen are also observed. We also plot the electron localization function (ELF) [39,40] and

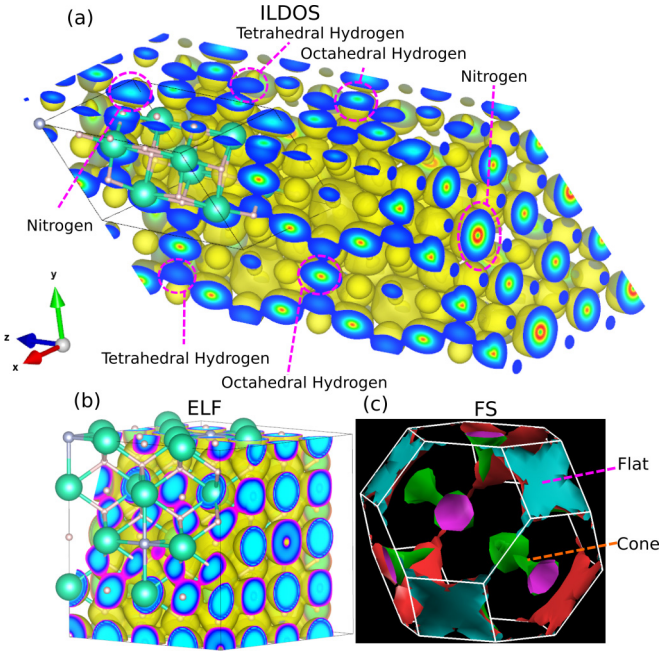

FIG. 4. Calculated local bonding and electronic properties for $Lu_8H_{23}N$ (A), with DFT+U, U on Lu_d of 8.2 eV. (a) Integrated local density of states (ILDOS), integrated ±5 meV from E_F. (b) The ELF, illustrating the formation of the hydrogen bonding network. (c) Fermi surface (FS).

find that the hydrogen ELF spheres begin to overlap at an isovalue of 0.51. While this hydrogen network has larger H-H distances of 2.15 Å that are larger than hydrides with highest T_c (0.9–1.35 Å) [13–16,36], the critical ELF isovalue of 0.51 is near that of LaH_{10} (0.45) [41], and belongs to the bonding class identified [41] as "weak H interactions" which has the highest T_c's and EPC. Use of the correlation between ELF and T_c [41] gives a critical temperature in the 120 K range for this structure with the Quantum Espresso projections. Using maximally localized Wannier function [42] projections (Figs. S16 and S17), the networking-value T_c estimate [41] rises to 180 K with U and only drops to 165 K without U. The large supercells here preclude complete (e.g., Eliashberg) calculation of T_c given our limited computational resources. In addition, calculation of EPC for DFT+U is not implemented in the EPW code [43]. The EPC enhancement from vHs and flat bands at E_F found for other high-T_c superconductors [8,9,12] combined with the known large EPC of FCC RH_3 [27] suggests that the band structure characteristics of $Lu_8H_{23-x}N$ phases predicted here support the existence of strong EPC (and thus very high T_c). The vHs peak of structure A near E_F is sharper than that of other high-T_c hydride superconductors (Fig. S19), with U enhancing this effect.

We briefly comment on the topological character of band structures found for these $LuH_{3-x}N_y$ phases. We first confirm that $Fm\bar{3}m$ LuH_3 has vHs and Dirac cones near E_F and is thus a potential Dirac semimetal, in agreement with recent calculations of Sufyan and Larsson [29]. The incorporation of N to form $Lu_8H_{23}N$ (A) shifts those topological features of LuH_3 2 eV above E_F (see Fig. S7). The Fermi surface of $Lu_8H_{23}N$ (A) (Fig. 4) clearly shows flat band regions and conelike regions. The flat bands of $Lu_8H_{23}N$ (A) are intersected by other bands (Figs. 2, S10, and S18), which can result in nontrivial topology for the bands (such as a nonzero Chern number). This is a necessary ingredient for flat-band superconductivity with nonzero superfluid weight [44,45]. As spin-orbit coupling (SOC) can have nontrivial effects on the electronic structure, we note its effects on LuH_3 primarily gaps the Dirac cones above E_F [29] but does not change the Fermi surface. We find that including SOC had negligible effects on the properties of structure A (Fig. S20), and so we do not consider SOC effects in more depth here. The results are consistent with a recent study of $Lu_4H_{11}N$ which indicated that SOC led to band splitting but did not appreciably affect the Fermi surface [46]. The band structures found for these $LuH_{3-x}N_y$ phases also have interesting parallels with the flat bands predicted for certain dense hydrogen structures of [47]. Nearly flat bands can emerge in multiband tight-binding models [48,49] due to geometric hybridization effects on idealized Kagome, Lieb, and checkerboard lattices [50]. These structures all share the trait of being highly symmetric, like those considered here. The nearly flat bands of $Lu_8H_{23}N$ (A) (Figs. 2 and S10) likely arise from the relative phases of the hopping parameter, and are further flattened with DFT+U (Fig. S18).

Finally, our results have important implications for experimental studies of the reported near-ambient superconductivity in the Lu-H-N system [1]. The sensitivity of the electronic properties in $Lu_8H_{23-x}N$ based phases to nitrogen and hydrogen-vacancy ordering suggests that emergent phenomena will be highly dependent on sample preparation and annealing. In addition, our calculated diffraction patterns should help guide experimental studies of the crystal structure (Fig. S6). We also note that the temperature dependence of the electrical resistance reported for Lu-H-N samples [1] shows striking parallels to anomalous resistivity curves documented many years ago for other substoichiometric lanthanide trihydrides (LnH_{3-x}) across their metal-insulator transitions [51,52] (Fig. S14), where the electrical conductivity has been shown to be strongly dependent on hydrogen-vacancy ordering [53].

In summary, we have identified classes of structures, stoichiometries, and hydrogen-vacancy ordering schemes for Lu-H-N with remarkable electronic properties. Our study predicts structures in the Lu-H-N system that match the experimental data [1] with electronic properties amenable to superconductivity, for which there is additional evidence from recently reported electrical resistance measurements [54]. We predict that structures A–D have predominantly hydrogen states at E_F and that strong correlations in structure A enhance the flat band character at E_F, which in turn is expected to enhance EPC [8,9]. We also predict that the proposed structures will exhibit interesting correlated physics, in addition to their potential for superconductivity, due to their flat bands at E_F. One of our goals was to inspire further theoretical and experimental work guided by the class of Lu-N-H structures we have found. Indeed, recent theoretical investigations [46,55,56] also reported sharp DOS peaks near E_F for structures similar to those studied here (i.e., with N in octahedral sites). With the method used to estimate T_c in Refs. [46,56], we find a T_c of 200 K for structure A. Moreover, recently reported

angle-resolved photoemission measurements [57] appear to confirm the remarkably flat bands and sharp vHs near E_F that we calculate and support the class of structures we predict for the material. Further tests of our predictions await detailed single-crystal x-ray and neutron diffraction and additional electron and x-ray spectroscopic measurements.

This research was supported by the NSF (DMR-2104881) and DOE-NNSA through the Chicago/DOE Alliance Center (DE-NA0003975; A.D. and R.H.), and NSF SI2-SSE Grant 1740112 (H.P.). We gratefully acknowledge the computing resources provided on Bebop, a high-performance computing cluster operated by the Laboratory Computing Resource Center at Argonne National Laboratory. This research used resources of the National Energy Research Scientific Computing Center (NERSC), a U.S. Department of Energy Office of Science User Facility located at Lawrence Berkeley National Laboratory, operated under Contract No. DE-AC02-05CH11231 using NERSC Award No. BES-ERCAP0023615.

[1] R. Dias, N. Dasenbrock-Gammon, E. Snider, R. McBride, H. Pasan, D. Durkee, N. Khalvashi-Sutter, S. Dissanayake, K. Lawler, and A. Salamat, Observation of room temperature superconductivity in hydride at near ambient pressure, Bull. Am. Phys. Soc. 68, Session #K20.0002 (2023).

[2] Z. Huo, D. Duan, T. Ma, Z. Zhang, Q. Jiang, D. An, H. Song, F. Tian, and T. Cui, First-principles study on the superconductivity of N-doped *fcc*-LuH_3, Matter Radiat. Extremes **8**, 038402 (2023).

[3] K. P. Hilleke, X. Wang, D. Luo, N. Geng, B. Wang, F. Belli, and E. Zurek, Structure, stability, and superconductivity of N-doped lutetium hydrides at kbar pressures, Phys. Rev. B **108**, 014511 (2023).

[4] P. P. Ferreira, L. J. Conway, A. Cucciari, S. Di Cataldo, F. Giannessi, E. Kogler, L. T. F. Eleno, C. J. Pickard, C. Heil, and L. Boeri, Search for ambient superconductivity in the Lu-N-H system, Nat. Commun. **14**, 5367 (2023).

[5] T. Lu, S. Meng, and M. Liu, Electron-phonon interactions in LuH_2, LuH_3, and LuN, arXiv:2304.06726.

[6] Y. Sun, F. Zhang, S. Wu, V. Antropov, and K.-M. Ho, Effect of nitrogen doping and pressure on the stability of LuH_3, Phys. Rev. B **108**, L020101 (2023).

[7] R. Lucrezi, P. P. Ferreira, M. Aichhorn, and C. Heil, Temperature and quantum anharmonic lattice effects on stability and superconductivity in lutetium trihydride, Nat. Commun. **15**, 441 (2024).

[8] W. Sano, T. Koretsune, T. Tadano, R. Akashi, and R. Arita, Effect of van Hove singularities on high-T_c superconductivity in H_3S, Phys. Rev. B **93**, 094525 (2016).

[9] T.-T. Gai, P.-J. Guo, H.-C. Yang, Y. Gao, M. Gao, and Z.-Y. Lu, Van Hove singularity induced phonon-mediated superconductivity above 77 K in hole-doped SrB_3C_3, Phys. Rev. B **105**, 224514 (2022).

[10] N. W. Ashcroft, Metallic hydrogen: A high-temperature superconductor? Phys. Rev. Lett. **21**, 1748 (1968).

[11] N. W. Ashcroft, Hydrogen dominant metallic alloys: High temperature superconductors? Phys. Rev. Lett. **92**, 187002 (2004).

[12] H. Liu, I. I. Naumov, R. Hoffmann, N. W. Ashcroft, and R. J. Hemley, Potential high-T_c superconducting lanthanum and yttrium hydrides at high pressure, Proc. Natl. Acad. Sci. USA **114**, 6990 (2017).

[13] F. Peng, Y. Sun, C. J. Pickard, R. J. Needs, Q. Wu, and Y. Ma, Hydrogen clathrate structures in rare earth hydrides at high pressures: Possible route to room-temperature superconductivity, Phys. Rev. Lett. **119**, 107001 (2017).

[14] M. Somayazulu, M. Ahart, A. K. Mishra, Z. M. Geballe, M. Baldini, Y. Meng, V. V. Struzhkin, and R. J. Hemley, Evidence for superconductivity above 260 K in lanthanum superhydride at megabar pressures, Phys. Rev. Lett. **122**, 027001 (2019).

[15] A. P. Drozdov, P. P. Kong, V. S. Minkov, S. P. Besedin, M. A. Kuzovnikov, S. Mozaffari, L. Balicas, F. F. Balakirev, D. E. Graf, V. B. Prakapenka, E. Greenberg, D. A. Knyazev, M. Tkacz, and M. I. Eremets, Superconductivity at 250 K in lanthanum hydride under high pressures, Nature (London) **569**, 528 (2019).

[16] E. Snider, N. Dasenbrock-Gammon, R. McBride, X. Wang, N. Meyers, K. V. Lawler, E. Zurek, A. Salamat, and R. P. Dias, Synthesis of yttrium superhydride superconductor with a transition temperature up to 262 K by catalytic hydrogenation at high pressures, Phys. Rev. Lett. **126**, 117003 (2021).

[17] P. Kong, V. S. Minkov, M. A. Kuzovnikov, A. P. Drozdov, S. P. Besedin, S. Mozaffari, L. Balicas, F. F. Balakirev, V. B. Prakapenka, S. Chariton, D. A. Knyazev, E. Greenberg, and M. I. Eremets, Superconductivity up to 243 K in the yttrium-hydrogen system under high pressure, Nat. Commun. **12**, 5075 (2021).

[18] I. A. Troyan, D. V. Semenok, A. G. Kvashnin, A. V. Sadakov, O. A. Sobolevskiy, V. M. Pudalov, A. G. Ivanova, V. B. Prakapenka, E. Greenberg, A. G. Gavriliuk, I. S. Lyubutin, V. V. Struzhkin, A. Bergara, I. Errea, R. Bianco, M. Calandra, F. Mauri, L. Monacelli, R. Akashi, and A. R. Oganov, Anomalous high-temperature superconductivity in YH_6, Adv. Mater. **33**, 2006832 (2021).

[19] K. P. Hilleke and E. Zurek, Tuning chemical precompression: Theoretical design and crystal chemistry of novel hydrides in the quest for warm and light superconductivity at ambient pressures, J. Appl. Phys. **131**, 070901 (2022).

[20] F. Xie, T. Lu, Z. Yu, Y. Wang, Z. Wang, S. Meng, and M. Liu, Lu-H-N phase diagram from first-principles calculations, Chin. Phys. Lett. **40**, 057401 (2023).

[21] W. Kohn and L. J. Sham, Self-consistent equations including exchange and correlation effects, Phys. Rev. **140**, A1133 (1965).

[22] P. Giannozzi, S. Baroni, N. Bonini, M. Calandra, R. Car, C. Cavazzoni, D. Ceresoli, G. L. Chiarotti, M. Cococcioni, I. Dabo, A. D. Corso, S. de Gironcoli, S. Fabris, G. Fratesi, R. Gebauer, U. Gerstmann, C. Gougoussis, A. Kokalj, M. Lazzeri, L. Martin-Samos *et al.*, QUANTUM ESPRESSO: A modular and open-source software project for quantum simulations of materials, J. Phys.: Condens. Matter **21**, 395502 (2009).

[23] P. Giannozzi, O. Andreussi, T. Brumme, O. Bunau, M. B. Nardelli, M. Calandra, R. Car, C. Cavazzoni, D. Ceresoli, M. Cococcioni, N. Colonna, I. Carnimeo, A. D. Corso, S. de Gironcoli, P. Delugas, R. A. DiStasio, A. Ferretti, A. Floris, G. Fratesi, G. Fugallo *et al.*, Advanced capabilities for materials modelling with QUANTUM ESPRESSO, J. Phys.: Condens. Matter **29**, 465901 (2017).

[24] Y.-C. Wang, Z.-H. Chen, and H. Jiang, The local projection in the density functional theory plus U approach: A critical assessment, J. Chem. Phys. **144**, 144106 (2016).

[25] S. A. Tolba, K. M. Gameel, B. A. Ali, H. A. Almossalami, and N. K. Allam, The DFT+U: Approaches, accuracy, and applications, in *Density Functional Calculations-Recent Progresses of Theory and Application*, edited by G. Yang (IntechOpen, London, UK, 2018), Chap. 1, Vol. 5772.

[26] P. Allen and R. Dynes, Superconductivity at very strong coupling, J. Phys. C **8**, L158 (1975).

[27] S. Villa-Cortés and O. De la Peña-Seaman, Superconductivity on ScH_3 and YH_3 hydrides: Effects of applied pressure in combination with electron-and hole-doping on the electron–phonon coupling properties, Chin. J. Phys. **77**, 2333 (2022).

[28] See Supplemental Material at http://link.aps.org/supplemental/10.1103/PhysRevMaterials.8.L021801 for a description of the computational methods, various additional calculations on the systems studied in the main text and comparisons of our theoretical results to other studies of hydrides. It also contains Ref. [58–68].

[29] A. Sufyan and J. A. Larsson, Topological nodal surface and quadratic Dirac semimetal states and van Hove singularities in ScH_3 and LuH_3 superconductors, ACS Omega **8**, 9607 (2023).

[30] M. Topsakal and R. Wentzcovitch, Accurate projected augmented wave (PAW) datasets for rare-earth elements (RE= La-Lu), Comput. Mater. Sci. **95**, 263 (2014).

[31] E. Cappelluti and L. Pietronero, Nonadiabatic superconductivity: The role of van Hove singularities, Phys. Rev. B **53**, 932 (1996).

[32] J. Bok and J. Bouvier, Superconductivity and the van Hove scenario, J. Supercond. Novel Magn. **25**, 657 (2012).

[33] J. Bardeen, L. N. Cooper, and J. R. Schrieffer, Theory of superconductivity, Phys. Rev. **108**, 1175 (1957).

[34] Y. Ge, F. Zhang, R. P. Dias, R. J. Hemley, and Y. Yao, Hole-doped room-temperature superconductivity in $H_3(S_{1-x}Z_x)$ (Z = C, Si), Mater. Today Phys. **15**, 100330 (2020).

[35] I. Errea, M. Calandra, C. J. Pickard, J. Nelson, R. J. Needs, Y. Li, H. Liu, Y. Zhang, Y. Ma, and F. Mauri, High-pressure hydrogen sulfide from first principles: A strongly anharmonic phonon-mediated superconductor, Phys. Rev. Lett. **114**, 157004 (2015).

[36] H. Liu, I. I. Naumov, Z. M. Geballe, M. Somayazulu, J. S. Tse, and R. J. Hemley, Dynamics and superconductivity in compressed lanthanum superhydride, Phys. Rev. B **98**, 100102(R) (2018).

[37] I. Errea, F. Belli, L. Monacelli, A. Sanna, T. Koretsune, T. Tadano, R. Bianco, M. Calandra, R. Arita, F. Mauri and J. A. Flores-Livas, Quantum crystal structure in the 250-kelvin superconducting lanthanum hydride, Nature (London) **578**, 66 (2020).

[38] K. K. Ly and D. M. Ceperley, Stability and distortion of fcc LaH_{10} with path-integral molecular dynamics, Phys. Rev. B **106**, 054106 (2022).

[39] A. Savin, R. Nesper, S. Wengert, and T. F. Fässler, ELF: The electron localization function, Angew. Chem. Int. Ed. Engl. **36**, 1808 (1997).

[40] P. Fuentealba, E. Chamorro, and J. C. Santos, Understanding and using the electron localization function, in *Theoretical and Computational Chemistry*, Vol. 19 (Elsevier, 2007), pp. 57–85.

[41] F. Belli, T. Novoa, J. Contreras-García, and I. Errea, Strong correlation between electronic bonding network and critical temperature in hydrogen-based superconductors, Nat. Commun. **12**, 5381 (2021).

[42] N. Marzari, A. A. Mostofi, J. R. Yates, I. Souza, and D. Vanderbilt, Maximally localized Wannier functions: Theory and applications, Rev. Mod. Phys. **84**, 1419 (2012).

[43] J. Noffsinger, F. Giustino, B. D. Malone, C.-H. Park, S. G. Louie, and M. L. Cohen, EPW: A program for calculating the electron-phonon coupling using maximally localized Wannier functions, Comput. Phys. Commun. **181**, 2140 (2010).

[44] S. Peotta and P. Törmä, Superfluidity in topologically nontrivial flat bands, Nat. Commun. **6**, 8944 (2015).

[45] M. Sato and Y. Ando, Topological superconductors: A review, Rep. Prog. Phys. **80**, 076501 (2017).

[46] N. S. Pavlov, I. R. Shein, K. S. Pervakov, V. M. Pudalov, and I. A. Nekrasov, Anatomy of the band structure of the newest apparent near-ambient superconductor $LuH_{3-x}N_x$, JETP Lett. **118**, 693 (2023).

[47] I. I. Naumov, R. E. Cohen, and R. J. Hemley, Graphene physics and insulator-metal transition in compressed hydrogen, Phys. Rev. B **88**, 045125 (2013).

[48] K. Sun, Z. Gu, H. Katsura, and S. Das Sarma, Nearly flat bands with nontrivial topology, Phys. Rev. Lett. **106**, 236803 (2011).

[49] D. Leykam, A. Andreanov, and S. Flach, Artificial flat band systems: From lattice models to experiments, Adv. Phys.: X **3**, 1473052 (2018).

[50] M. Kang, S. Fang, L. Ye, H. C. Po, J. Denlinger, C. Jozwiak, A. Bostwick, E. Rotenberg, E. Kaxiras, J. G. Checkelsky, and R. Comin, Topological flat bands in frustrated kagome lattice CoSn, Nat. Commun. **11**, 4004 (2020).

[51] J. Shinar, B. Dehner, R. G. Barnes, and B. J. Beaudry, Anomalous resistivity peaks, localization transitions, and the electronic structure of substoichiometric lanthanum trihydrides, Phys. Rev. Lett. **64**, 563 (1990).

[52] G. Libowitz, Electronic properties of the rare earth hydrides, Ber. Bunsenges. Phys. Chem. **76**, 837 (1972).

[53] T. C. Kerscher, G. Schöllhammer, P. Herzig, W. Wolf, R. Podloucky, and S. Müller, First-principles study of hydrogen ordering in lanthanum hydride and its effect on the metal-insulator transition, Phys. Rev. B **86**, 014107 (2012).

[54] N. P. Salke, A. C. Mark, M. Ahart, and R. J. Hemley, Evidence for near ambient superconductivity in the Lu-N-H system, arXiv:2306.06301.

[55] W. Wu, Z. Zeng, and X. Wang, Investigations of pressurized Lu-N-H materials by using the hybrid functional, J. Phys. Chem. C **127**, 20121 (2023).

[56] Y.-W. Fang, Đ. Dangić, and I. Errea, Assessing the feasibility of near-ambient conditions superconductivity in the Lu-N-H system, arXiv:2307.10699.

[57] X. Liang, Z. Lin, J. Zhang, J. Zhao, S. Feng, W. Lu, G. Wang, L. Shi, N. Wang, P. Shan, Z. Zhang, M. Naamneh, R. Liu, B.

Michon, J. Cheng, C. Jin, Y. Ren, and J. Ma, Observation of flat band and van Hove singularity in nitrogen doped lutetium hydride, arXiv:2308.16420.

[58] G. Prandini, A. Marrazzo, I. E. Castelli, N. Mounet, and N. Marzari, Precision and efficiency in solid-state pseudopotential calculations, npj Comput. Mater. **4**, 72 (2018).

[59] A. Dal Corso, Pseudopotentials periodic table: From H to Pu, Comput. Mater. Sci. **95**, 337 (2014).

[60] S. P. Ong, W. D. Richards, A. Jain, G. Hautier, M. Kocher, S. Cholia, D. Gunter, V. L. Chevrier, K. A. Persson, and G. Ceder, Python materials genomics (pymatgen): A robust, open-source python library for materials analysis, Comput. Mater. Sci. **68**, 314 (2013).

[61] M. Kawamura, Y. Gohda, and S. Tsuneyuki, Improved tetrahedron method for the Brillouin-zone integration applicable to response functions, Phys. Rev. B **89**, 094515 (2014).

[62] K. Momma and F. Izumi, VESTA 3 for three-dimensional visualization of crystal, volumetric and morphology data, J. Appl. Cryst. **44**, 1272 (2011).

[63] Q. Wu, S. Zhang, H.-F. Song, M. Troyer, and A. A. Soluyanov, WannierTools: An open-source software package for novel topological materials, Comput. Phys. Commun. **224**, 405 (2018).

[64] D. Chakraborty, K. Berland, and T. Thonhauser, Next-generation nonlocal van der Waals density functional, J. Chem. Theory Comput. **16**, 5893 (2020).

[65] M. Schlipf, M. Betzinger, C. Friedrich, M. Ležaić, and S. Blügel, HSE hybrid functional within the FLAPW method and its application to GdN, Phys. Rev. B **84**, 125142 (2011).

[66] K. Niwa, M. Hasegawa, and T. Yagi, Synthesis of Ln nitrides (Ln = Ce, Pr, Gd, Lu) in high pressure and temperature, J. Alloys Compd. **477**, 493 (2009).

[67] M. Liu, X. Liu, J. Li, J. Liu, Y. Sun, X.-Q. Chen, and P. Liu, On parent structures of near-ambient nitrogen-doped lutetium hydride superconductor, Phys. Rev. B **108**, L020102 (2023).

[68] J. Shinar, B. Dehner, B. J. Beaudry, and D. T. Peterson, Q-factor measurements of the bulk resistivity and nonmetal-metal transitions in LaH_x and CeH_x ($x \geqslant 2.70$), Phys. Rev. B **37**, 2066 (1988).